Change of the unbinding mechanism upon a mutation: A molecular dynamics study of an antibody–hapten complex

RAFFAELE CURCIO, AMEDEO CAFLISCH, AND EMANUELE PACI
Biochemisches Institut der Universität Zürich, CH-8057 Zürich, Switzerland

(RECEIVED December 8, 2004; FINAL REVISION April 1, 2005; ACCEPTED April 11, 2005)

Abstract

We study forced unbinding of fluorescein from the wild type (WT) and a mutant [H(H58)A] of the single-chain variable-fragment (scFv) anti-fluorescein antibody FITC-E2 by molecular dynamics simulations using various pulling techniques. A large number of long simulations were needed to obtain statistically meaningful results as both the wild type and the H(H58)A mutant unbinding occurs through multiple pathways, often with metastable intermediates. For the wild type, the rate-limiting step in the unbinding process corresponds to the breaking of the non-native interactions characteristic of a specific intermediate. The H(H58)A mutation disfavors the occurrence of this intermediate. Two events where the hapten partially unbinds in the absence of pulling force are observed in extensive equilibrium simulations of the wild type, and their analysis indicates that forced unbinding and spontaneous unbinding proceed along similar pathways. The different unbinding mechanisms observed in the simulations suggest a possible reason for the difference in the experimental off-rate between the two antibodies. We predict mutations that are expected to modulate the occurrence of the unbinding intermediate. For two such new mutants [H(H58)A and S(H52)A], our predictions are validated in silico by additional simulations. The accompanying paper in this issue by Honegger et al. reports the X-ray structure of FITC-E2 with a derivative of fluorescein, which was used as the starting conformation for the work presented here.

Keywords: molecular dynamics; atomic force microscopy; forced unbinding; antibody–hapten complex; non-native interactions

Molecular recognition is essential for many biochemical processes such as enzyme reactions (Fersht 1999), recognition of DNA sequences by regulatory proteins, protein–protein or protein–ligand recognition (Kleanthous 2000; Wodak and Janin 2002), and drug design (Doucet and Weber 1996). To understand how specific recognition is achieved, it is important to know the underlying mechanisms of the binding and unbinding processes.

In this respect, atomic force microscopy (AFM) is a valuable tool to shed light on the unbinding mechanism of a biological complex on the single-molecule level, removing the averaging over large ensembles of molecules implied in other biophysical/biochemical approaches. Two different AFM techniques are available to probe the mechanical resistance of biomolecules: in the force-ramp method, a time-dependent force is applied (Florin et al. 1994), while in the so-called force-clamp method, the force is held constant (Oberhauser et al. 2001). Based on the force-ramp method, dynamic force spectroscopy (Evans and Ritchie 1997) has provided a deep insight into the unbinding mechanism of a variety of biological complexes, such as the (strept)avidin–biotin complex (Merkel et al. 1999) and the complex between L-selectin and various binding partners (Evans et al. 2001), providing details on the unbinding pathway.

However, it is desirable to relate the information provided by the AFM techniques on unbinding of a complex

Reprint requests to: Dr. Emanuele Paci, Institute of Molecular Biophysics, School of Physics and Astronomy, University of Leeds, Leeds LS2 9JT, UK; e-mail: e.paci@leeds.ac.uk; fax: +44-113-3433900.

Article and publication are at http://www.proteinscience.org/cgi/doi/10.1110/ps.041280705.

to the underlying molecular structure in order to gain an atomic-level description of the unbinding process. For this purpose, AFM observations can be complemented with molecular dynamics (MD) simulations, which also study the behavior of individual molecules. Steered MD (SMD) and constant force MD (CFMD) simulations mimic the force-ramp and the force-clamp methods of AFM, respectively, and have been widely used to study unbinding (Grubmüller et al. 1996; Izrailev et al. 1997; Heymann and Grubmüller 1999, 2001; Paci et al. 2001) and protein unfolding (Lu et al. 1998; Paci and Karplus 1999, 2000; Isralewitz et al. 2001). Although AFM experiments and SMD/CFMD simulations study a process at greatly different time scales, since the former are typically carried out on the millisecond time scale or slower while the latter are currently limited to nanoseconds, the computational approach has generated several predictions subsequently verified by experiments and explained experimental observations (Evans and Ritchie 1997; Lu et al. 1998; Krammer et al. 1999; Marszalek et al. 1999; Fowler et al. 2002; Best et al. 2003; Brockwell et al. 2003; Carrion-Vazquez et al. 2003).

In this paper, we present a simulation study of the forced unbinding process of the wild type (WT) and a mutant [H(H58)A] of the single-chain variable-fragment (scFv) anti-fluorescein antibody FITC-E2, which has been experimentally studied by the AFM technique (Ros et al. 1998; Schwesinger et al. 2000). The experiment determined loading-rate-dependent unbinding forces that extrapolated at zero force to a value close to the thermal off-rate measured in solution. Moreover, the measured unbinding forces for nine different scFv anti-fluorescein antibodies (three unrelated fragments and some of their single point mutants) correlated with the off-rate in solution, leading to the conclusion that spontaneous unbinding and forced unbinding proceed through very similar unbinding pathways.

The results presented in this paper have been obtained by performing a large number of independent forced unbinding simulations, using both steered and constant force molecular dynamics, and in the latter case using forces of various magnitudes. The approach provides a statistically relevant picture of the unbinding mechanism. It also provides an indication on the robustness of the results to the variation of the pulling technique that forces the unbinding in the simulations. We chose to use an approximate implicit description of the solvent (Lazaridis and Karplus 1999), which allowed us to explore much longer time scales (we performed a total of $\sim$2.5 μsec, including equilibrium and forced unbinding simulations for the various species). However, the simulation of forced unbinding, even using simpler models, is limited to a few nanoseconds when many independent simulations need to be performed. For this reason, the pulling speed that has to be used in the SMD simulations must be several orders of magnitude larger than the experimental one. As unbinding forces strongly depend on the loading rate (or pulling speed), the primary interest of the present study is not to predict the experimentally measured unbinding force, but to describe the mechanism of forced unbinding of two antibody–antigen complexes at the atomic level and to understand the differences between the wild-type complex and various mutants.

In both the wild-type and the H(H58)A complexes, forced unbinding proceeded along multiple pathways. However, only in the case of the wild type, the unbinding pathway often passes through a particularly stable conformation, stabilized mainly by non-native interactions. This finding could explain the increase of the rate of spontaneous unbinding upon the H(H58)A mutation observed in the experiments (Schwesinger et al. 2000) if one assumes that forced unbinding and spontaneous unbinding occur along similar pathways. In two partial unbinding events at zero pulling force observed in extensive equilibrium simulations (600 nsec in total) of the wild-type complex, the hapten changes its position reaching a binding mode structurally very similar to the stable conformation frequently detected in the forced unbinding simulations. This finding suggests that forced and spontaneous unbinding might, indeed, occur through a very similar mechanism.

A conformational analysis of the binding pocket, and of the pathways of forced unbinding, suggested mutations of FITC-E2 expected to modulate the preference for the unbinding pathway passing through (or avoiding) the stable intermediate. For two such new mutations [H(H58)W and S(H52)A], forced unbinding simulations were performed and confirmed our predictions about the unbinding pathways. The possible effect of the H(H58)W and S(H52)A mutations on the unbinding rate of the FITC-E2 fluorescein complex is also discussed.

The present study clearly indicates that unbinding might be a complicated multistep process involving the formation and breaking of non-native interactions between the two binding partners of a complex.

Results

Control runs

Long equilibrium simulations (60 nsec) were performed with the wild-type and the H(H58)A mutant complex to test the quality of the force field and solvation model used as well as the starting conformation (which, for the mutant, has been modeled as described in the Materials and Methods section). The structure of the wild-type scFv antibody FITC-E2 in complex with fluorescein is

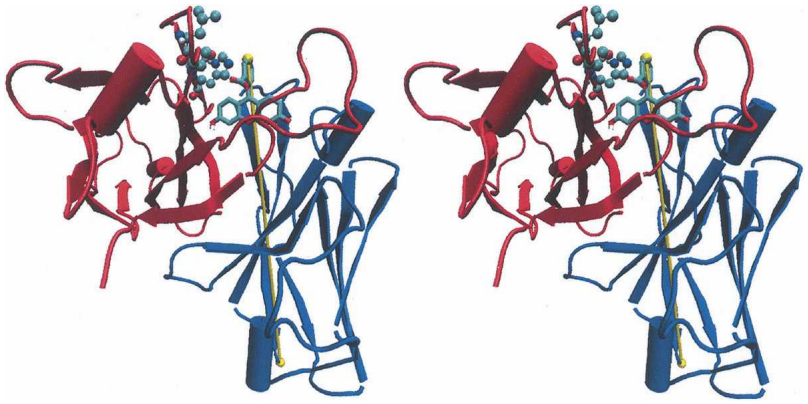

Figure 1. Stereo image of the X-ray structure of the FITC-E2 (Honegger et al. 2005) complexed to fluorescein. The antibody's light and heavy chains are colored blue and red, respectively, and the residues in sticks are S(H52), L(H56), and H(H58). The yellow line connecting the fluorescein and the antibody atoms represents the vector r_{FA}, that is, the direction of the applied force. The figure was generated with VMD (Humphrey et al. 1996).

shown in Figure 1. It consists of two variable domains, V_L and V_H, connected by the linker $(G\text{-}G\text{-}G\text{-}G\text{-}S)_3$. In this study, the effect of the linker was modeled by adding a harmonic restraint on the distance between the N terminus of V_L and the C terminus of V_H. The overall structure of the wild-type antibody is well conserved over the 60 nsec of the control run (see Fig. 2A). In contrast, in the case of the H(H58)A mutant, three solvent-exposed heavy chain strands, far away from the binding pocket and mutually interacting, lose some of their contacts with the rest of the chain and fluctuate. However, the C_α-RMSD time series determined without taking into account these strands (19 out of 126 residues, eight of them being C-terminal residues) shows that the rest of the antibody structure was well conserved over the control run also for the mutant. The fluorescein maintains its position within the binding pocket over the whole control run for both the wild type and the H(H58)A mutant (see Fig. 2B,C). Moreover, almost all the contacts between the hapten and the antibody present in the initial structure, also referred to as native hapten–antibody contacts, are preserved: the fraction of native antibody–fluorescein contacts Q_{native} (see Materials and Methods) is close to one throughout the entire control run (Fig. 2D). The averages of Q_{native} and of the other quantities shown in Figure 2 over the part of the control run from which the conformations were extracted to start the forced unbinding simulations are given in Table 1.

The stability observed in these long control runs indicates that the force field and the implicit solvation model are accurate and appropriate for this system. One main advantage of implicit relative to explicit solvation models is that they make it possible to perform much longer simulations. In a simulation of a different antibody–hapten complex using explicit solvent (Heymann and Grubmüller 2001), the stability of the hapten within the binding pocket over a 1.5-nsec simulation is comparable to our results with the implicit solvent over a 60-nsec time scale.

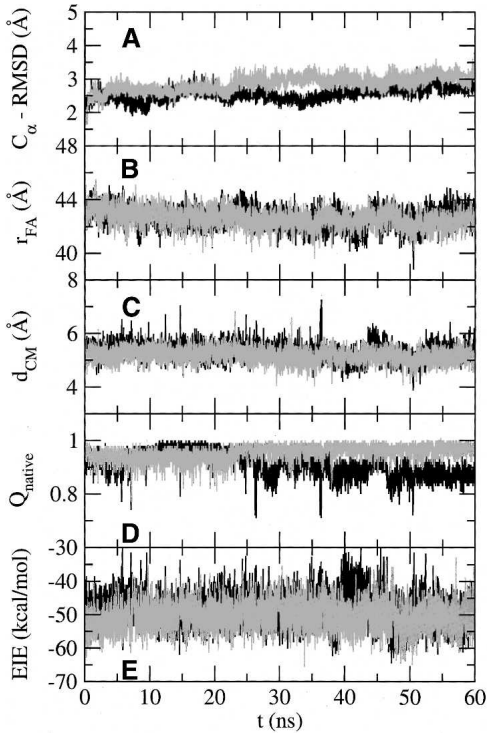

Figure 2. Time series along the control run of the wild type (black line) and the H(H58)A mutant of FITC-E2 (gray line) of (*A*) the root mean square deviation (RMSD) of the C_α atoms of FITC-E2 (light plus heavy chain) from the X-ray structure (for the mutant some residues were left out, see text); (*B*) distance between the two atoms pulled apart in the forced unbinding simulations (r_{FA}); (*C*) distance between the center of mass of fluorescein and of the binding pocket (d_{cm}); (*D*) fraction of native antibody–fluorescein contacts (Q_{native}); (*E*) effective antibody–fluorescein interaction energy (EIE).

Table 1. *Data from the 60-nsec control run of the WT, the H(H58)A, the H(H58)W, and the S(H52)A mutant of FITC-E2*

	WT	H(H58)A	H(H58)W	S(H52)A
C_α-RMSD (Å)	2.5 ± 0.2	3.4 ± 0.3	3.2 ± 0.2	3.1 ± 0.2
r_{FA} (Å)	42.6 ± 0.7	42.5 ± 0.6	41.2 ± 0.6	42.7 ± 0.6
d_{cm} (Å)	5.3 ± 0.3	5.2 ± 0.3	5.1 ± 0.3	5.4 ± 0.2
Q_{native}	0.91 ± 0.05	0.97 ± 0.02	0.93 ± 0.03	0.82 ± 0.03
EIE (kcal/mol)	−48.7 ± 4.6	−49.9 ± 4.2	−50.7 ± 3.5	−50.6 ± 3.8

All values were averaged over the second third of the control run. r_{FA} is the distance between the two atoms pulled apart in the forced unbinding simulations; d_{cm} is the distance between the center of mass of fluorescein and the binding pocket; Q_{native} is the fraction of native antibody–fluorescein contacts; EIE is the effective antibody-fluorescein interaction energy (see Materials and Methods for the exact definitions).

The native interactions between fluorescein and the binding pocket residues, i.e., the ones found in the X-ray structure of the complex (Honegger et al. 2005), are shown in Figure 3. For both the wild type and the H(H58)A mutant, the strong van der Waals interaction between the hapten and W(L91), the buried hydrogen

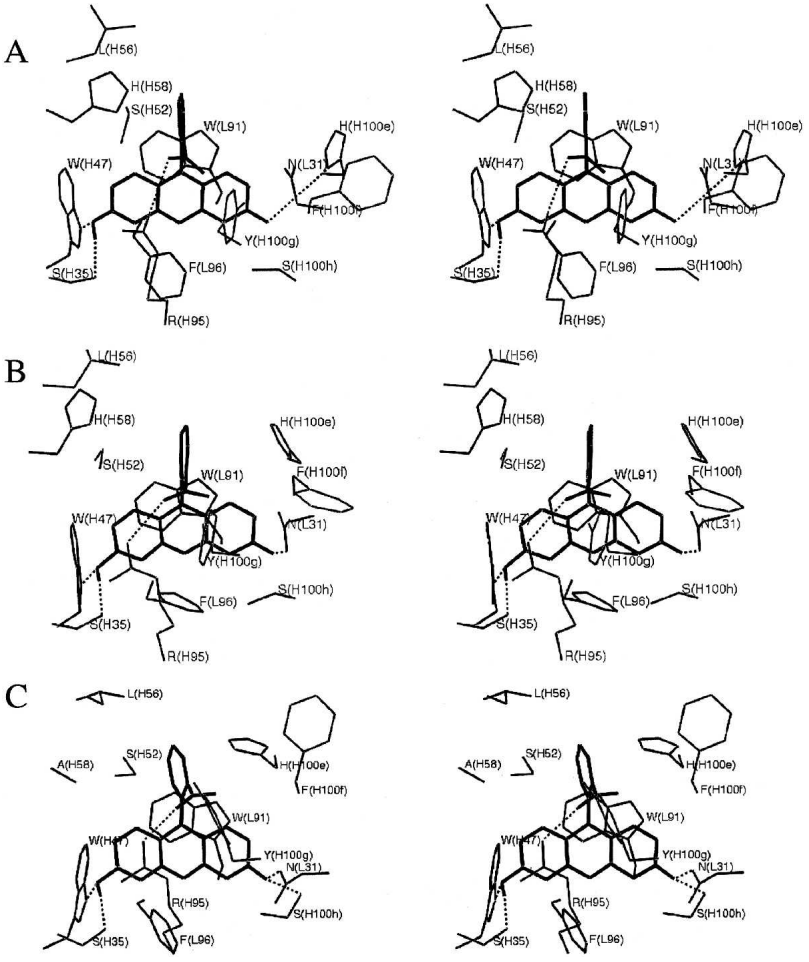

Figure 3. Stereo image of the structure of the binding pocket of FITC-E2 in complex with fluorescein (thick lines) in (*A*) the X-ray structure, and in a representative snapshot of the control run of (*B*) the wild type and (*C*) the H(H58)A mutant, respectively. Only antibody residues (thin lines) contacting the hapten are shown (see Table 2) together with the hydrogen bonds involving the hapten (dotted lines).

Table 2. *Average effective interaction energy ($\langle E_{eff} \rangle$) for fluorescein and antibody residues contacting the hapten*

Antibody residue	No. of native contacts	$\langle E_{eff} \rangle$ (kcal/mol)
S(H35)	8	–4.9 ± 1.6 (–4.2 ± 1.9)
W(H47)	48	–4.3 ± 2.0 (–5.0 ± 1.5)
S(H52)	9	–1.7 ± 0.8 (–1.2 ± 0.9)
L(H56)	2	0.0 ± 0.1 (–0.4 ± 0.9)
H(H58) (A(H58))	51 (7)	–1.2 ± 0.9 (–0.1 ± 0.1)
R(H95)	82	–6.5 ± 1.4 (–6.8 ± 1.4)
H(H100e)	13	–3.0 ± 1.0 (–2.6 ± 0.7)
Y(H100g)	10	–3.0 ± 0.9 (–3.3 ± 0.7)
S(H100h)	4	–1.8 ± 1.5 (–5.8 ± 2.0)
N(L31)	7	–3.8 ± 2.1 (–3.6 ± 0.9)
W(L91)	137	–8.4 ± 1.1 (–7.9 ± 1.0)
F(L96)	42	–3.4 ± 0.9 (–3.2 ± 0.8)

Energies were averaged over the second third of the control run. Quantities in brackets refer to the H(H58)A mutant. For the definition of the native contacts, see Materials and Methods.

bonds [with S(H35) and W(H47)], and the strong salt bridge with R(H95) are conserved along the control runs of both the wild type and the mutant (see Fig. 3B,C and Table 2). In contrast, the native hydrogen bond between the hapten and H(H100e), which is partly exposed to the solvent (see Fig. 3A), was sometimes broken; the hydrogen bond to this histidine was replaced by one to N(L31) during the control run of both systems, while it was only in the case of the mutant, that a buried hydrogen bond with S(H100h) was formed and persisted until the end of that control run (see Fig. 3B,C and Table 2). Apart from this non-native strong hydrogen bond with S(H100h), the hapten–antibody interaction pattern was very similar and the total fluorescein–antibody interaction energy was approximately constant and of the same magnitude for the wild type and the mutant over the entire control run (see Fig. 2E and Table 1). Interestingly, in the wild type, residue H(H58) was only marginally stabilizing for the hapten in its native binding mode (see Table 2). This solvent-exposed residue was found to change interaction partners in the long control run, often forming a hydrogen bond with the spatially close S(H52) side chain.

Forced unbinding of the wild type and the H(H58)A mutant

SMD simulations

Figure 4 shows the typical force time series for two SMD simulations for each of the two FITC-E2 species. Peaks in the applied force reflect the presence of a barrier related to the rupture of antibody–hapten interactions. The initial peak reflects the rupture of the native antibody–hapten interactions. A second peak is often observed for both species, which reveals the presence of a metastable state along the forced unbinding pathway. In the case of the mutant, the initial force peak is always the highest. For the wild type instead, in 5/20 forced unbinding simulations the second peak was found to be higher than the first one (see Fig. 4A).

Owing to the compliance of the cantilever (i.e., the harmonic spring that is retracted at constant speed in the SMD simulations) and of the antibody, the distance between hapten and antibody does not increase linearly with time; it will increase more slowly when barriers are encountered (while the applied force increases) and more quickly when the barriers are overcome (while the applied force drops). The presence of barriers can thus be inferred from the double peak in the histogram of the distance between the center of mass of fluorescein and

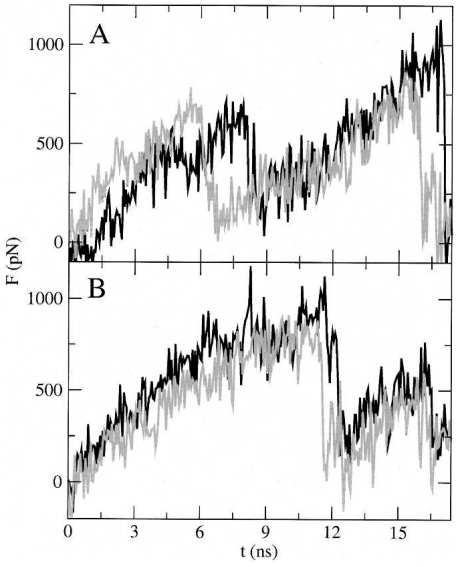

Figure 4. Two typical force time series of the SMD simulations of unbinding of (*A*) the wild type and (*B*) the H(H58)A mutant.

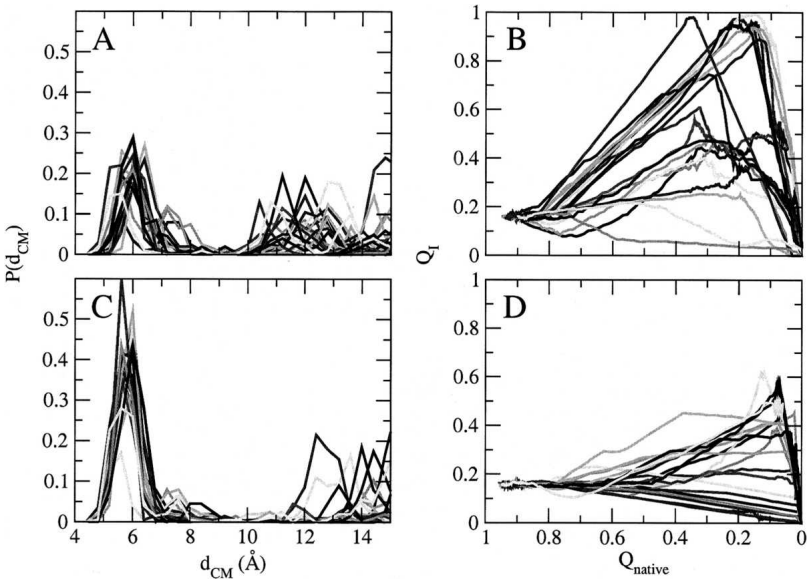

Figure 5. Histograms of d_{cm} and the fraction of antibody–hapten contacts in I_{WT} (Q_I, see text) as a function of Q_{native} for the 20 SMD simulations of (*A*,*B*) the wild type and (*C*,*D*) the H(H58)A mutant, respectively. Forced unbinding starts in the lower left-hand corner and proceeds from the *left* to the *right* in the plots *B* and *D*.

the center of mass of the binding pocket (d_{cm}; see Materials and Methods) in Figure 5, A and C, the first peak (at a $d_{cm} \approx 5.5$ Å) reflecting the relative persistence in the bound state. For the wild type, all runs showed the presence of barriers, while for the H(H58)A mutant only sometimes. The occurrence of a barrier is related to the existence of a state that is metastable, i.e., an intermediate under the applied force; this appears even more clearly in the analysis of the CFMD simulations presented in the next section.

Visual inspection of the forced unbinding runs reveals the existence of multiple unbinding pathways. Figure 6, A and B, shows the binding mode of fluorescein in the most frequently observed bottlenecks for the wild type and the mutant, respectively. The binding mode represented by the conformation shown in Figure 6A, which we call here "intermediate of the wild type" (I_{WT}), corresponds to a state that is stable over a considerable time even under the effect of the pulling force. The conformation I_{WT} is particularly relevant, because the difference between the unbinding pathways of the two species consists in the fact that the wild type often passes through I_{WT}, while the H(H58)A mutant never does. This can be clearly seen from the plots of the fraction of antibody–hapten contacts in I_{WT} (Q_I) against the fraction of native contacts (see Fig. 5B,D). Similarly to Q_{native}, Q_I is defined as the fraction of the contacts of the intermediate present in a given conformation. The contacts of the intermediate I_{WT} were determined by computing the average distances between heavy atoms of the hapten and the antibody for a set of conformations extracted from the five SMD simulations for which the distribution of d_{cm} has the highest second peak; a cutoff of 6 Å on the average distance was used to define the contacts. The same analysis done with five suitable CFMD runs (see below) yields an identical set of antibody–fluorescein contacts in I_{WT}. In the case of the wild type, 8/20 runs show a maximum of Q_I higher than 0.8, that is, pass through I_{WT}, while all runs of the mutant have no Q_I larger than 0.65. In both binding modes shown in Figure 6, the hapten is involved in non-native interactions with the antibody, in particular, a hydrogen bond with R(H95). But while in the binding mode shown in Figure 6B fluorescein is nearly outside the binding pocket (at a $d_{cm} \approx 12$–14 Å) (see Fig.5C), in I_{WT} fluorescein is still within the binding pocket (at a $d_{cm} \approx 10$–12 Å) (see Fig. 5A), strongly interacting with the antibody. In fact, the five runs of the wild type with a second barrier higher than the first one all pass through I_{WT}, the second barrier reflecting the rupture of the non-native interactions strongly stabilizing I_{WT}.

The bottlenecks or intermediates observed in the other SMD runs (six for the wild type and 14 for the mutant) vary structurally from simulation to simulation, but are all short-lived.

CFMD simulations

In CFMD simulations the externally applied force decreases the height of the free energy barriers along the direction of the force, thus making it possible to

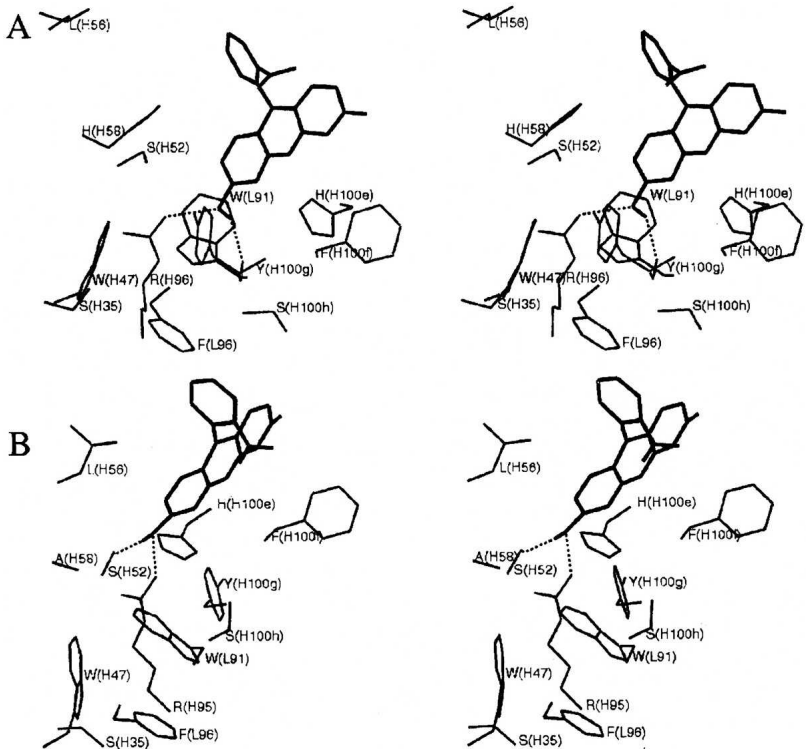

Figure 6. Stereo image of the binding mode of fluorescein in the most frequently observed forced unbinding intermediate of the SMD simulations of (*A*) the wild type and (*B*) the H(H58)A mutant.

observe the thermally activated crossing of the barrier on the short time scales accessible by simulation (Bell 1978; Evans 2001). For a simple two-state process, the logarithm of the average unbinding time decreases linearly with the applied force. For both the wild type and the H(H58)A mutant, 20 simulations at three different forces between 300 and 400 pN were performed (see Materials and Methods). In all cases, simulations were continued until total unbinding occurred. In the limited range of forces explored, the logarithm of the unbinding time is effectively linear in the applied force (data not shown), for both the wild type and H(H58)A.

The time series of d_{cm} for two unbinding simulations using a constant force of 300 pN is shown in Figure 7, A and B, for the wild type and the H(H58)A mutant, respectively. The behavior is typical of a thermally activated barrier crossing. In the two cases shown for the mutant, the unbinding occurs through the crossing of a single barrier, while in the cases shown for the wild type, the unbinding occurs through the crossing of an additional barrier. One advantage of constant forced unbinding simulations, as for unfolding simulations (Fowler et al. 2002), is that metastable states and transitions between them can be detected more easily from the observation of traces such as shown in Figure 7A and that metastable states can be stabilized on long time scales. For the wild type, forced unbinding events with and without intermediates are observed, the latter being quite rare (with a force of 300 pN only one run over 20).

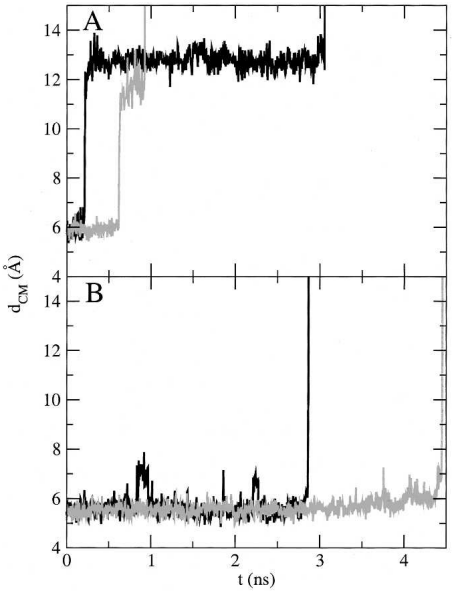

Figure 7. Typical behavior of d_{cm} as a function of the time shown for two CFMD simulations of (*A*) the wild type and (*B*) the H(H58)A mutant. The force used to induce unbinding was 300 pN.

For the H(H58)A mutant, intermediates are never observed in the forced unbinding simulations at 300 and 350 pN force; at large force, 400 pN, we observe another regime where unbinding occurs very fast and the mechanism of unbinding is slightly different; a bottleneck very close to the initial one at $d_{cm} \approx 7$–8 Å is observed in five out of 20 simulations. In the case of the mutant, the strong perturbation induced by such a high force affects the unbinding pathways. However, in the case of the wild-type system, the unbinding pathways are more robust, and very similar to those observed with the SMD method even when unbinding is induced by a 400-pN constant force.

In particular, the second barrier clearly evident in the CFMD simulations for the unbinding of the wild-type complex from the traces shown in Figure 7A corresponds to the passage through the intermediate I_{WT} described above, which is encountered frequently at each force. This appears clearly from Figure 8, where Q_I is shown as a function of Q_{native} for the CFMD simulations. At the lowest force (300 pN), for the wild type, in 10 out of 20 simulations the trajectory clearly passes through I_{WT}, while for the H(H58)A mutant, as observed before, this particular pathway is avoided at any force. The intermediate I_{WT} can be best characterized from the CFMD run shown in Figure 7A, where this metastable state is maintained for nearly 3 nsec. CFMD simulations clearly show that, at least in the range of forces explored, the rate-limiting step in the unbinding of fluorescein from the wild-type antibody corresponds to the breaking of the interactions that stabilize I_{WT}. On the contrary, for the H(H58)A mutant, the rate-limiting step corresponds to the breaking of the native interactions between the binding partners.

Most likely pathway of forced unbinding

We present here a "consensus picture" of the most frequently observed unbinding pathway and of the common features of the various unbinding pathways observed. For both the wild type and the H(H58)A mutant, at the beginning of the forced unbinding process, the strong native interactions between the fluorescein and the binding pocket residues, and in particular the salt bridge with R(H95) (see Fig. 3A), enable the hapten to withstand the external force. The hapten does not move from its initial position and the interaction pattern is conserved, while in the SMD simulations the applied force quickly increases as the cantilever is retracted (see Fig. 4). However, after a small displacement of the hapten from its initial position within the binding pocket, all native interactions with the antibody break, except the salt bridge with R(H95). This salt bridge is the last native interaction to break in many forced unbinding simulations of both the wild type and the H(H58)A mutant (16/20 SMD runs and 12/20 CFMD runs at 300 pN for the wild type; 13/20 SMD runs and 10/20 CFMD runs at 300 pN for the mutant). This is probably due to the strength of this interaction but most likely also to the flexibility of the arginine's side chain, which allows R(H95) to better respond to small displacements of the hapten than other binding pocket residues. The importance of salt bridges in determining the tensile strength of a complex

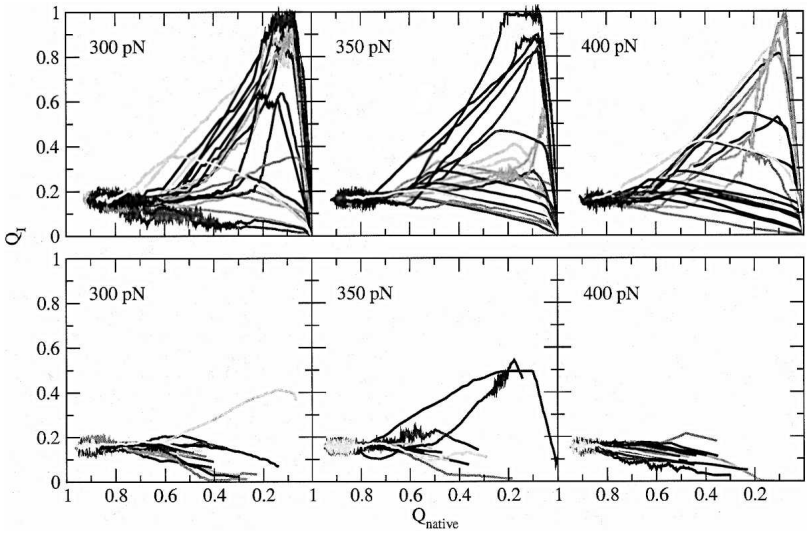

Figure 8. Q_I as a function of Q_{native} for the 20 CFMD simulations of the wild type (*upper* part) and of the H(H58)A mutant (*lower* part) for the three forces used to induce unbinding.

has been also stressed by Schulten and coworkers (Bayas et al. 2003).

In the case of the wild type, this small displacement of the hapten is followed by a rotation of the fluorescein within the binding pocket accompanied by a translation in direction of the V_L domain. This rotational and translational movement of fluorescein within the binding pocket was observed in all forced unbinding simulations of the wild-type system passing through I_{WT}.

In the case of the mutant, no hapten rotation or translation within the binding pocket is observed in any run; instead, fluorescein is always steered along the direction of the applied force, often directly exiting the binding pocket. Instead, for the wild type, the unbinding intermediate I_{WT} is frequently formed after the rupture of the native antibody–hapten interactions.

Also in I_{WT} (see Fig. 6A), residue R(H95) interacts with fluorescein but through a non-native strong hydrogen bond with the xanthenone hydroxy group, which is also hydrogen-bonded to a backbone atom of residue Y(H100g); these two strong non-native interactions anchor fluorescein in a new position within the binding pocket. Apart from the two anchoring hydrogen bonds, there are other interactions stabilizing this intermediate, most of them being non-native ones. Interestingly, the residues H(H100e), F(H100f), and Y(H100g), whose mutation into an alanine increases the off-rate compared to the wild type (Schwesinger et al. 2000), are also found to interact with fluorescein in I_{WT}. While H(H100e) and F(H100f) are only involved in van der Waals interactions, Y(H100g) forms also a hydrogen bond with the hapten in that intermediate, explaining the different mean effective interaction energy found for these residues in I_{WT} from the CFMD run shown in Figure 7A [–2.76 (±1.12) kcal/mol and –3.81 (±1.49) kcal/mol for H(H100e) and F(H100f), but –7.04 (±1.74) kcal/mol for Y(H100g)]. It is worth mentioning, that F(H100f) has zero native contacts with the hapten and only marginally interacts with it in the bound state. This can be seen from Figure 9, where the interaction between the fluorescein and selected residues of the wild-type antibody interacting with the hapten at some stage of the SMD runs of the unbinding process is shown as a function of Q_{native}.

There are also other residues almost exclusively involved in non-native interactions in a late stage of the forced unbinding process and not contributing to the stability of the bound state, for example, S(L95a) (often hydrogen-bonded to fluorescein in I_{WT}), showing that most of the antibody-fluorescein interactions in any forced unbinding intermediate are non-native ones. After the breaking of the anchoring interactions, the hapten is free to exit the binding pocket of the wild-type antibody.

In conclusion, the H(H58)A mutation is found to change the preference for pathways of forced unbinding by avoiding a particular pathway with a major bottleneck (represented by the escape from I_{WT}) and to favor the exploration of a variety of other pathways, which augments the heterogeneity of forced unbinding pathways as compared to the wild type.

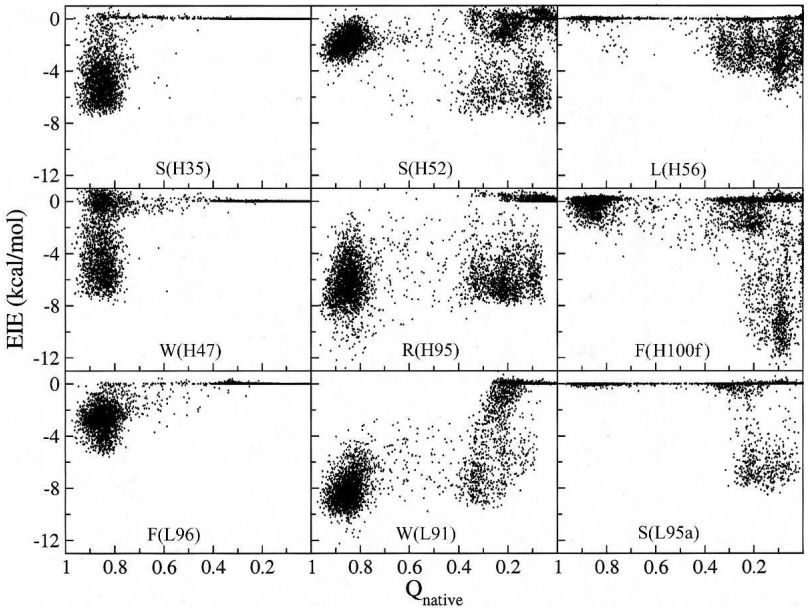

Figure 9. Effective interaction energy (EIE) between fluorescein and some antibody residues as a function of Q_{native} in the forced unbinding process of the wild type. All 20 SMD simulations were taken into account (first column, residues with native contacts only; second column, residues with native and non-native contacts; third column, residues with mostly non-native contacts).

Spontaneous displacement of fluorescein from the wild-type complex

The control simulations showed that the antibody–fluorescein complexes are stable at 300 K over 60 nsec. In an attempt to gain insight into the mechanism of spontaneous unbinding and in the spirit of the distributed computing approach (Pande et al. 2003), we performed several (20) simulations 30 nsec long at 300 K for the wild type and the H(H58)A complexes by assigning different initial velocities (see Materials and Methods). While in the case of the mutant, fluorescein maintained its native binding mode in all the simulations, in two wild-type runs, partial unbinding of fluorescein (d_{cm} never increases beyond 14 Å) in the absence of a pull ing force was observed. Interestingly, in the partial unbinding events, the fluorescein ends up in the intermediate I_{WT} observed in the forced unbinding. This is evident from Figure 10, A and B, where Q_I is plotted as a function of Q_{native}: the hapten clearly moves, through discrete jumps, from the original binding mode to an alternative one that corresponds to I_{WT} and remains there until the simulation is stopped. Detailed analysis of these trajectories shows that as in forced unbinding of the wild type, the formation of I_{WT} was preceded by a rotation within the binding pocket and a translation of the hapten toward the V_L domain. Unbinding seems never to be a single step from the bound state.

These common features between spontaneous and forced unbinding suggest that forced and spontaneous unbinding of fluorescein occur along pathways that are remarkably similar (at least for the wild-type complex). In the next section, we investigate further the structural reason for the similarity of forced and spontaneous unbinding pathways.

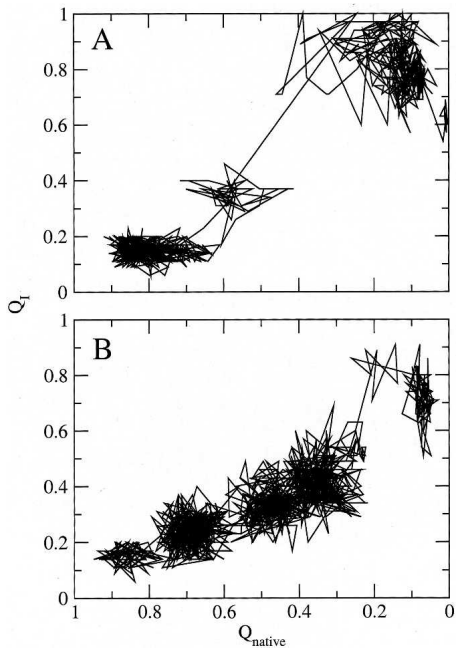

Figure 10. The two spontaneous partial unbinding events (*A* and *B*) observed for the wild type, shown as Q_I as a function of Q_{native}.

Prediction of the unbinding mechanism of new mutants

For the wild-type system, the forced unbinding process was frequently found to proceed through a specific intermediate (I_{WT}) (see Fig. 6A), not observed in any forced unbinding simulation of the H(H58)A mutant. From the crystal structure of the fluorescein–FITC-E2 complex, and in particular from the arrangement of the binding pocket residues around the hapten, it can be inferred that the applied force initially directs fluorescein against the side chain of three V_H domain residues [H(H58), S(H52), and L(H56)] (see Fig. 1). Residues H(H58) and S(H52) directly contact the hapten, while L(H56) does not. In the case of the wild type, this group of amino acids, and H(H58) and S(H52) in particular, occlude the way out of the antibody binding pocket along the direction of the external force. The control runs of the wild type and the H(H58)A mutant showed that these three heavy-chain residues (in positions 52, 56, and 58) maintain all their native contacts with the hapten and their positional fluctuations are small. In addition, in the case of the wild type, a non-native hydrogen bond between the side chains of H(H58) and S(H52) is often present in the control run (47% of the time). This non-native hydrogen bond involves two residues that are in contact with the hapten and further hinders fluorescein on its way out of the binding pocket in the direction of the applied force, forcing the fluorescein through an alternative way out of the binding pocket as schematically represented in Figure 11A. In both forced and spontaneous unbinding, this process starts with a rotation within the binding pocket and a translation of the hapten toward the V_L domain, away from the three residues mentioned above. This rotational and translational movement frequently ends up with the formation of the intermediate I_{WT}.

The H(H58)A mutation removes the large imidazole ring and reduces considerably the steric hindrance experienced by fluorescein during the forced unbinding process. This mutation therefore facilitates the unbinding of fluorescein from the antibody in direction of the applied force, that is, through an alternative route compared to the wild type (see Fig. 11B). Although it cannot be excluded, it is reasonable to assume that the passage through I_{WT} in the unbinding process, mainly induced by H(H58) in the case of the wild type, is avoided upon the H(H58)A mutation also in the absence of any external force.

The presence of the unbinding intermediate I_{WT} in the forced and the spontaneous process could then be corre-

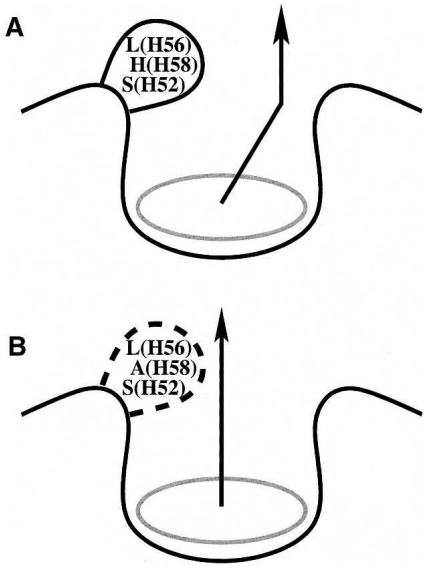

Figure 11. Model of the binding pocket for (*A*) the wild type and (*B*) the H(H58)A mutant, respectively. The dashed segment (in panel *B*) indicates the reduced steric hindrance in the case of the H(H58)A mutant in that position of the binding pocket. The hapten is represented by the gray ellipse and the hapten's way out of the binding pocket by the arrowed line.

lated to the extent of the steric hindrance caused by the binding pocket residues in positions H52 and H58 (and H56 to a smaller extent). Thus the mutation of these residues is expected to vary the preference for the unbinding pathway passing through I_{WT}, the H(H58)A mutant completely avoiding it.

To verify this hypothesis, we studied the unbinding mechanism of two additional mutants, S(H52)A and H(H58)W, by means of SMD simulations. The former mutation is expected to reduce the steric hindrance and therefore the likelihood for the presence of I_{WT}. For the latter mutation, the opposite is expected.

Control runs of the S(H52)A and H(H58)W mutants

As for the wild type and the H(H58)A mutant, we performed long control simulations to assess the stability of the complexes involving the S(H52)A and H(H58)W mutants. The overall structure of the two mutants and the position of the hapten in the binding pocket were conserved over the control runs. In particular, quantities such as r_{FA}, d_{cm}, and Q_{native} show no drift, and their average values over the control run are shown in Table 1. As for the H(H58)A mutant, the average C_α-RMSD for the H(H58)W and the S(H52)A mutants is slightly higher than that for wild type because of a rearrangement of solvent-exposed heavy chain segments (13 and 14 residues for the former and the latter mutant, respectively) far from the binding pocket. For the S(H52)A mutant, the fraction of native contacts in the binding pocket (Q_{native}) decreases to 0.82, mainly due to a rearrangement of the H(H58) side chain. As mentioned, in the control run of the wild type, residue H(H58) makes a stable non-native hydrogen bond with its neighbor S(H52). The mutation S-to-A prevents the formation of this hydrogen bond, and the side chain of H(H58) moves away from A(H52) and the hapten to form a hydrogen bond with the backbone oxygen of Y(H59).

In the case of the H(H58)W mutant, no rearrangement of the residue W(H58) and its structural neighbors was observed. The hydrogen bond between W(H58) and S(H52) modeled in the starting structure of this mutant was conserved over the entire control run. As for the wild type and the H(H58)A mutant, the native but solvent-exposed hydrogen bond between the xanthenone hydroxy group and H(H100e) breaks, while stable non-native interactions between that hapten site and the antibody are formed also during the control run of the H(H58)W and the S(H52)A mutant. The formation of a non-native hydrogen bond with N(L31) was observed in the case of the H(H58)W mutant, while such an interaction was found to involve S(H100h) in the case of the S(H52)A mutant. Apart from these two non-native interactions, the hapten–antibody interaction pattern observed in the control runs was very similar for the two mutants.

Forced unbinding simulations of the H(H58)W and S(H52)A mutants

All forced unbinding simulations of the H(H58)W mutant showed the presence of an intermediate corresponding to $d_{cm} \approx 10$–14 Å (see Fig. 12A) as in the case of the wild type, and in most cases the peak of the force at this value of d_{cm} is larger than the one corresponding to the exit from the initial bound state. More interesting, in 13 over 20 runs the unbinding pathway passes through I_{WT} (see Fig. 12B). This result confirms our expectation that the passage through I_{WT} would have been frequently observed, even more than for the wild type, owing to the effect of the increased steric hindrance introduced by the mutation.

For the S(H52)A mutant, most unbinding pathways proceeded through short-lived intermediates, similarly to the H(H58)A mutant (see Fig. 12C). In all cases, the first peak in the force time series is the highest, indicating that the main barrier is related to the breaking of the native antibody–hapten interactions. As expected, the structural changes in the binding pocket due to the S(H52)A mutation reduce the likelihood to pass through I_{WT}, relative to the wild type. However, in three out of 20 simulations, unbinding was still found to proceed through I_{WT} (see Fig. 12D). The fact that in the case of

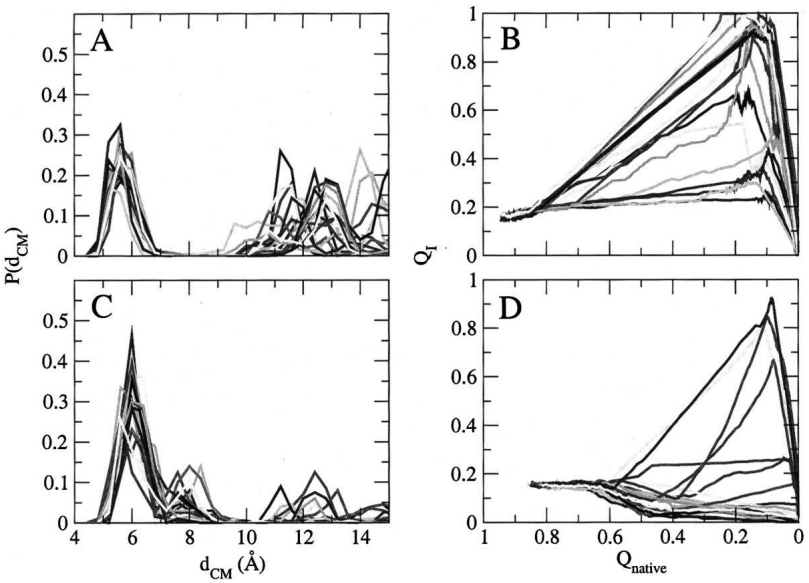

Figure 12. Histograms of d_{cm} and Q_I as a function of Q_{native} for the 20 SMD simulations of (*A*,*B*) the H(H58)W and (*C*,*D*) the S(H52)A mutant of FITC-E2, respectively.

the S(H52)A the passage through I_{WT} is sometimes observed while never in the H(H58)A, is probably related to the considerably larger structural change that the latter mutation introduce in the binding pocket region.

Discussion

The results presented above provide a rational base for interpreting in microscopic terms the unbinding mechanism of a hapten–antibody complex. For the fluorescein–FITC-E2 complex and several of its mutants, experimental off-rates in solution have been measured as well as the single-molecule unbinding force (Schwesinger et al. 2000). The experiment pointed out that off-rates and unbinding forces correlate and thus the mechanical force needed to extract the hapten from the antibody provides a measure of the antibody–hapten affinity, the equilibrium on-rates being nearly constant (Schwesinger et al. 2000). We focused here on the wild type and the H(H58)A mutant for which the experimentally measured increase in off-rate was largest (~100-fold).

For both species, multiple pathways are observed in the forced unbinding simulations. A heterogeneity of forced unbinding pathways rather than a single well-defined one was also found in other computational studies of forced processes (Grubmüller et al. 1996; Izrailev et al. 1997; Heymann and Grubmüller 2001; Paci et al. 2001; Bayas et al. 2003).

Although some similarities in the forced unbinding mechanism of the two species are observed, the H(H58)A mutation significantly changes the preference for certain pathways. While for the wild type, forced unbinding frequently proceeds through a pathway with a particular intermediate or bottleneck (called here I_{WT}), the mutant always avoids this pathway. This intermediate is stabilized by mostly non-native interactions with the antibody. As suggested by the force time series of the SMD simulations and, even more clearly, by the center-of-mass distance time series in CFMD simulations, in a considerable fraction of trajectories the rate-limiting step corresponds to the breaking of the non-native interactions stabilizing I_{WT}. In contrast, in the case of the mutant, the main barrier always corresponds to the breaking of the interactions present in the bound state.

The presence of an unbinding intermediate is in apparent contradiction with the related AFM experiment of Schwesinger et al. (2000). The presence of multiple barriers along the pathway of unbinding was excluded because of the linear dependence of the unbinding force on the logarithm of the loading rate (which is the product of the force constant by the pulling speed) for the wild-type complex (Schwesinger et al. 2000). However, in the experiments, the loading rate dependence of the unbinding force was measured over only two orders of magnitude in loading rate. This might not be sufficient to detect a deviation from linearity indicating the presence of multiple barriers along the pathway of unbinding (Merkel et al. 1999). It is worth stressing

that in the limited force range of our constant force simulations, despite the multiple pathways and multiple barriers observed, the logarithm of the mean unbinding time decreases linearly with the applied force.

The behavior of the wild-type and H(H58)A complexes in the absence of an external pulling force has been studied by performing many long simulations starting from the bound state. For the wild-type complex, in two out of 20 simulations the hapten changes its original binding mode and assumes an alternative stable position relative to the antibody. This binding mode is identical to the critical bottleneck (I_{WT}) frequently observed in the forced unbinding pathway. This finding suggests that at lower pulling speed the population of the intermediate might be an obligatory step, and that forced and spontaneous unbinding might effectively proceed through identical pathways as suggested by the experiment (Schwesinger et al. 2000). Provided that also in the case of the mutant the mechanisms of forced and spontaneous unbinding are similar, our simulations give a plausible explanation of the observed off-rate increase upon the H(H58)A mutation of FITC-E2.

As suggested by the rather small favorable interaction between the side chain of H(H58) and the hapten in the bound structure and along the control run, the acceleration of the spontaneous process upon the H(H58)A mutation observed experimentally might not be related to the breaking of crucial interactions in the binding pocket introduced by the mutation. Instead, faster unbinding might originate from the ability of the mutant to avoid the pathway through an intermediate more stable than the bound state (Wagner and Kiefhaber 1999).

The different unbinding mechanisms (presence/absence of I_{WT}) for wild type and H(H58)A can be related to the structural features of the binding pocket and, in particular, to the key position assumed by residues S(H52), L(H56), and H(H58). These residues are found to sterically hinder the hapten on its way out of the binding pocket of the wild-type antibody, regardless of the loading rate (i.e., for forced and spontaneous unbinding). Our simulations have shown that the pathway to circumvent this hindrance in the unbinding process often proceeds through I_{WT}. The mutation H(H58)A significantly reduces the extent of this hindrance that forces the hapten through that particular unbinding route in the case of the wild type. This mutation can thus be assumed to facilitate a direct exit of the hapten out of the binding pocket after the rupture of the native interactions even in the absence of an external force.

Based on the unbinding mechanisms observed for the wild type and the H(H58)A mutant, the effect on the off-rate of published mutations can be rationalized. The residues H(H100e), F(H100f), and Y(H100g), whose mutation into an alanine accelerates unbinding as compared to the wild type (Schwesinger et al. 2000), all interact through their side chains with the hapten in I_{WT}. The H(H100e)A, F(H100f)A, and Y(H100g)A mutations remove this favorable interaction in I_{WT}, leading to an early rate-limiting step, similarly to the situation of the H(H58)A mutant, rationalizing the experimental observations related to the off-rate. The residue L(H56) belongs to the group of residues sterically hindering the hapten during unbinding and should therefore favor the presence of the long-lived intermediate I_{WT}. The L(H56)A mutation reduces the extent of that steric hindrance and can thus be expected to reduce the occurrence of I_{WT} in the unbinding process, leading to a faster unbinding. An increased off-rate was, indeed, experimentally observed for this mutant of FITC-E2. Interestingly, this residue and F(H100f) do not interact directly with the hapten in the bound state, yet they influence the kinetics of unbinding.

In the same line, other mutations can be suggested that either affect the stabilization of I_{WT} or favor its presence/absence in the unbinding process and thus affect the off-rate. Mutations like F(H100f)Y and S(L95a)A are expected to modify the kinetic stability of I_{WT} as compared to the wild type. Also S(L95a) interacts with fluorescein in I_{WT} forming a hydrogen bond, while F(H100f) interacts through a van der Waals interaction. The proposed mutations should enable/disable the formation of a hydrogen bond with the hapten in I_{WT}, increasing/decreasing its kinetic stability as compared to the wild type and leading to a slower/faster unbinding. Mutations like H(H58)W and S(H52)A both modify the extent of the abovementioned steric hindrance experienced by fluorescein during unbinding. The H(H58)W mutation enlarges this hindrance as compared to the wild type and should therefore favor the presence of I_{WT} even more than the wild type itself. The S(H52)A mutation is expected to have the opposite effect on the unbinding mechanism. Our predictions have been validated in silico by forced unbinding simulations of the modeled H(H58)W and S(H52)A mutants. Provided that the presence of I_{WT} slows down the process of unbinding and that the forced and the spontaneous processes are similar for all these FITC-E2 species, the S(H52)A mutation is expected to accelerate, whereas the H(H58)W mutation is expected to slow down unbinding as compared to the wild type. It would be particularly interesting to study the effect of a double mutation on the off-rate, for instance, of H(H58)W/F(H100f)Y. The more frequently formed intermediate I_{WT} [due to the H(H58)W mutation] is better stabilized [due to the F(H100f)Y mutation] than in the case of the wild type. This could slow down unbinding more than the two single mutations alone.

For the five FITC-E2 mutants studied by Schwesinger et al. (2000)—L(H56)A, H(H58)A, H(H100e)A, F(H100f)A,

and Y(H100g)A—the ϕ values for unbinding can be estimated as

$$\phi^{unb} = \ln \frac{k^{off}_{mut}}{k^{off}_{WT}} / \ln \frac{K^{D}_{mut}}{K^{D}_{WT}},$$

where i is the mutated residue, k^{off}_{mut} and k^{off}_{WT} are the off-rates, and K^{D}_{mut} and K^{D}_{WT} the dissociation constants of the mutant and the wild type, respectively. ϕ values are a measure of the change in the free energy barrier relative to the change in stability upon mutation, that is, $\phi^{unb} = \Delta\Delta_r G_{TS-B}/\Delta\Delta_r G_{U-B}$, where B, TS, and U represent the bound, transition, and unbound states, respectively, and the first Δ means the difference between the mutant antibody and wild type. In the simplest and most widely used interpretation, ϕ values are related to the fraction of native (bound) contacts present in the transition state (Fersht 1999; Lindorff-Larsen et al. 2003). ϕ values have been broadly used to characterize the transition state for folding of two-state proteins and more recently also to study the binding process of such a large complex as a TCR–pMHC complex (Wu et al. 2002). A novel approach (Vendruscolo et al. 2001; Paci et al. 2002) extends the information that can be obtained from experimental ϕ values by using simulation to generate high-resolution models of the transition state. This approach could have, in principle, been used to determine the transition state for fluorescein–FITC-E2 unbinding. However, only a small number of ϕ^{unb} is available, and two of them are larger than 1 [1.7 and 1.5 for the H(H58)A and the L(H56)A mutations, respectively] and therefore not suited to classical interpretation of these quantities (Fersht 1999). Moreover, simulation shows that unbinding is a complicated, multistep process involving the formation and breaking of non-native interactions that makes the ϕ^{unb} unsuitable for the interpretation as the fraction of native contacts. Interestingly, the two mutations giving rise to nonclassical ϕ values of unbinding both reduce the steric hindrance experienced by fluorescein during unbinding and favor the absence of the important bottleneck represented by I_{WT} in the unbinding process, as shown by our forced unbinding simulations of the H(H58)A mutant.

Materials and methods

MD simulations were performed with the CHARMM program (Brooks et al. 1983) using an all-atom model of the protein and an implicit model for the solvent (EEF1) (Lazaridis and Karplus 1999) that provides a potential-of-mean-force description of the solvent. While explicit solvation models are in general more accurate, in the specific case of forced unbinding simulations, it has been previously argued (Paci and Karplus 2000) that when large conformational changes are forced to occur in a very short time compared to the experiment, the relaxation of an explicit solvent might be too slow and add artifacts. The implicit solvent model used guaranteed the stability of the complex over a 60-nsec time scale (see Results).

The X-ray structure of the wild type FITC-E2 complexed to a derivative of fluorescein (Honegger et al. 2005) was used as starting conformation for the simulations, thereby the fluorescein analog in the X-ray structure was replaced with fluorescein itself. The structure of the H(H58)A mutant of the antibody was generated by removing the imidazole group of the residue H(H58) in the X-ray structure of the wild type (as in Schwesinger et al. 2000); the numbering of the residues follows the rules of Kabat et al. (1987). The determination of suitable force-field parameters for the hapten is described in detail elsewhere (Paci et al. 2001).

The structures of the wild type and the H(H58)A mutant were energy-minimized with 100 steps of steepest descent, followed by 1000 steps of conjugate-gradient algorithm. The systems were then gradually heated from 10 K to 300 K in 2-K steps every 6 psec for a total of 870 psec and then equilibrated at 300 K for 130 psec by reassigning the velocities when the temperature deviated by more than 30 K. During this phase of heating and equilibration, the position of all backbone atoms of the two structures was constrained by applying a harmonic force. This was followed by another 1-nsec unconstrained simulation in the microcanonical ensemble, where the translational and rotational movements of the complexes were stopped every 2 psec. As control run, for each species, the simulation was continued in the canonical ensemble for another 60 nsec using the Nosé-Hoover thermostat (Nosé 1984; Hoover 1985). The SHAKE algorithm (Ryckaert et al. 1977) was used to fix the length of the covalent bonds involving hydrogen atoms, which allowed an integration time step of 2 fsec in all simulations.

By assigning different starting velocities to the atoms of the two structures at the beginning of the heating phase and applying the same procedure described above, 20 independent 30-nsec simulations were performed for both complexes. The purpose of these additional runs, totaling 600 nsec per each complex, was to increase the probability of observing at least the initial phase of unbinding in the absence of a pulling force.

The conservation of the contacts between the hapten (fluorescein) and the antibody present in the experimental structure of the wild type [or in the minimized structure of the H(H58)A mutant], also referred to as native hapten–antibody contacts, was monitored throughout all equilibrium and forced unbinding runs. A quantity Q_{native} was defined as the fraction of native contacts present in a given conformation. Contacts are defined as the number of heavy atom pairs, one belonging to the fluorescein and the other to a side chain of the antibody, at a distance lower than 6 Å.

To induce the unbinding of fluorescein from the antibody, two different methods were applied: steered and constant force molecular dynamics. In both cases, an external force is applied to one atom of the antibody and one atom of the fluorescein. Since in the AFM experiments (Schwesinger et al. 2000) the antibody (A) is immobilized through the carboxyl C-atom of the light chain's C-terminal residue on a gold surface while the retracting cantilever is attached to the C-2 atom of fluorescein (F), the same pairs of atoms are pulled apart in the forced unbinding simulations. Thus the applied force is directed as the vector joining the two atoms to which it is applied (r_{FA}; see Fig. 1).

In the SMD method the following time-dependent external force is applied:

$$F(t) = k[vt - (r_{FA}(t) - r_{FA}(0))] \quad (1)$$

where $v = 6$ Å/nsec corresponds to the velocity of the retracting cantilever and $k = 100$ pN/Å is its force constant. The value of v was chosen so that the complete unbinding of the hapten occurs within 5 nsec, that is, the total run length of each SMD simulation. The value of k was chosen to allow thermal fluctuation of r_{FA} in the range of the unperturbed value (~0.6 Å), according to $\delta r_{FA} = (k_B T/k)^{1/2}$, where δr_{FA} is the fluctuation of the r_{FA} distance, k_B is the Boltzmann constant, and T is the absolute temperature. The force constant k used here is ~10 times larger than the k of the experimental cantilever (Ros et al. 1998; Schwesinger et al. 2000), and the value of v is nearly six orders of magnitude higher than the experimental pulling speed.

The application of a constant force in single-molecule force spectroscopy is now experimentally possible and has been recently applied to study protein unfolding (Oberhauser et al. 2001; Fernandez and Li 2004). The application of a constant pulling force in simulation is straightforward and has been previously used to simulate forced unbinding (Paci et al. 2001) and unfolding (Fowler et al. 2002). In a CFMD simulation, the relaxation from the initial bound conformation to the equilibrium one, where ligand and antibody are at infinite distance, is monitored. The presence of a constant force has the effect of lowering the free energy barrier for the unbinding; the thermally activated crossing of the barriers can thus be observed over shorter time scales. To explore the effect of the magnitude of the force on the unbinding mechanism, three different forces (300, 350, and 400 pN) were used in the CFMD simulations. The magnitude of the force was chosen so that, with the smallest force (300 pN), unbinding still occurred on a time scale shorter than 15 nsec. All simulations were continued until unbinding occurred.

We selected 20 independent initial conformations of the two complexes, one each nanosecond, in the interval 21–40 nsec of the control runs. Then 20 unbinding simulations, starting from these initial conformations, were performed using SMD and CFMD, in the latter case for each of the three different constant forces employed. Thus, 80 unbinding events were observed for each complex studied.

Besides monitoring the increase of r_{FA}, unbinding was also monitored using quantities more specifically depending on the events taking place in the binding pocket of the antibodies in the course of a forced unbinding simulation. One is the distance between the center of mass of fluorescein and the center of mass of the binding pocket (d_{cm}), defined as the center of mass of the C_α atoms of six binding pocket residues. Another quantity is the fraction of native antibody–hapten contacts Q_{native} defined above.

Two additional mutants, H(H58)W and S(H52)A, were also modeled based on the X-ray structure of the wild type, as described for the H(H58)A mutant. In the case of the H(H58)W mutation, the tryptophan side chain was modeled such as to form a hydrogen bond to the nearby S(H52) side chain. Control runs and 20 SMD simulations were performed for these two mutants exactly as described for the wild type and the H(H58)A mutant.

Acknowledgments

We gratefully acknowledge Ch. Cambillau for providing the crystal structure previous to publication. We thank A. Honegger and A. Plückthun for useful discussions and critical reading of the manuscript. We also thank A. Widmer (Novartis Pharma, Basel) for providing the molecular modeling program Wit!P, which was used for visual analysis of the trajectories and to generate Figures 3 and 6. The simulations were performed on the Matterhorn Beowulf cluster at the Computing Center of the University of Zurich. We thank Ch. Bolliger, T. Steenbock, and A. Godknecht for setting up and managing the cluster and the Canton of Zurich for generous hardware support. This work was supported by the Swiss National Competence Center for Research (NCCR) in Structural Biology.

References

Bayas, M.V., Schulten, K., and Leckband, D. 2003. Forced detachment of the CD2–CD58 complex. *Biophys. J.* **84:** 2223–2233.

Bell, G.I. 1978. Models for the specific adhesion of cells to cells. *Science* **200:** 618–627.

Best, R.B., Fowler, S., Toca-Herrera, J.L., Steward, A., Paci, E., and Clarke, J. 2003. Mechanical unfolding of a titin Ig domain: Structure of transition state revealed by combining atomic force microscopy, protein engineering and molecular dynamics simulations. *J. Mol. Biol.* **330:** 867–877.

Brockwell, D.J., Paci, E., Zinober, R.C., Beddard, G.S., Olmsted, P.D., Smith, D.A., Perham, R.N., and Radford, S.E. 2003. Pulling geometry defines the mechanical resistance of a β-sheet protein. *Nat. Struct. Biol.* **10:** 731–737.

Brooks, B.R., Bruccoleri, R.E., Olafson, B.D., States, D.J., Swaminathan, S., and Karplus, M. 1983. CHARMM: A program for macromolecular energy, minimization and dynamics calculations. *J. Comp. Chem.* **4:** 187–217.

Carrion-Vazquez, M., Li, H., Lu, H., Marszalek, P.E., Oberhauser, A.F., and Fernandez, J.M. 2003. The mechanical stability of ubiquitin is linkage dependent. *Nat. Struct. Biol.* **10:** 738–743.

Doucet, J.-P. and Weber, J. 1996. *Computer-aided molecular design: Theory and applications*. Academic Press, London.

Evans, E. 2001. Probing the relation between force-lifetime and chemistry in single molecular bonds. *Annu. Rev. Biophys. Biomol. Struct.* **30:** 105–128.

Evans, E. and Ritchie, K. 1997. Dynamic strength of molecular adhesion bonds. *Biophys. J.* **72:** 1541–1555.

Evans, E., Leung, A., Hammer, D., and Simon, S. 2001. Chemically distinct transition states govern rapid dissociation of single L-selectin bonds under force. *Proc. Natl. Acad. Sci.* **98:** 3784–3789.

Fernandez, J.M. and Li, H. 2004. Force-clamp spectroscopy monitors the folding trajectory of a single protein. *Science* **303:** 1674–1678.

Fersht, A.R. 1999. *Structure and mechanism in protein science: A guide to enzyme catalysis and protein folding*. W.H. Freeman, New York.

Florin, E.L., Moy, V.T., and Gaub, H.E. 1994. Adhesion forces between individual ligand–receptor pairs. *Science* **264:** 415–417.

Fowler, S., Best, R.B., Toca-Herrera, J.L., Rutherford, T., Steward, A., Paci, E., Karplus, M., and Clarke, J. 2002. Mechanical unfolding of a titin Ig domain: Structure of unfolding intermediate revealed by combining AFM, molecular dynamics simulations, NMR and protein engineering. *J. Mol. Biol.* **322:** 841–849.

Grubmüller, H., Heymann, B., and Tavan, P. 1996. Ligand binding: Molecular mechanics calculation of the streptavidin-biotin rupture force. *Science* **271:** 997–999.

Heymann, B. and Grubmüller, H. 1999. AN02/DNP-hapten unbinding forces studied by molecular dynamics atomic force microscopy simulations. *Chem. Phys. Lett.* **303:** 1–9.

———. 2001. Molecular dynamics force probe simulations of antibody/antigen unbinding: Entropic control and nonadditivity of unbinding forces. *Biophys. J.* **81:** 1295–1313.

Honegger, A., Spinelli, S., Cambillau, C., and Plückthun, A. 2005. A mutation designed to alter crystal packing permits structural analysis of a tight-binding fluorescein–scFv complex. *Protein Sci.* **14:** 2537–2549.

Hoover, W.G. 1985. Canonical dynamics: Equilibrium phase-space distributions. *Phys. Rev. A* **31:** 1695–1697.

Humphrey, W., Dalke, A., and Schulten, K. 1996. VMD—Visual Molecular Dynamics. *J. Mol. Graphics* **14:** 33–38.

Isralewitz, B., Gao, M., and Schulten, K. 2001. Steered molecular dynamics and mechanical functions of proteins. *Curr. Opin. Struct. Biol.* **11:** 224–230.

Izrailev, S., Stepaniatis, S., Balsera, M., Oono, Y., and Schulten, K. 1997. Molecular dynamics study of unbinding of the avidin–biotin complex. *Biophys. J.* **72:** 1568–1581.

Kabat, E.A., Wu, T.T., Reid-Miller, M., Perry, H.M., and Gottesman, K.S. 1987. Sequences of proteins of immunological interest. *Technical*

report. US Department of Health and Human Services. National Institutes of Health, Bethesda, MD.
Kleanthous, C. 2000. *Protein–protein recognition*. Oxford University Press, Oxford.
Krammer, A., Lu, H., Isralewitz, B., Schulten, K., and Vogel, V. 1999. Forced unfolding of the fibronectin type III module reveals a tensile molecular recognition switch. *Proc. Natl. Acad. Sci.* **96:** 1351–1356.
Lazaridis, T. and Karplus, M. 1999. Effective energy function for protein dynamics and thermodynamics. *Proteins* **35:** 133–152.
Lindorff-Larsen, K., Paci, E., Serrano, L., Dobson, C.M., and Vendruscolo, M. 2003. Calculation of mutational free energy changes in transition states for protein folding. *Biophys. J.* **85:** 1207–1214.
Lu, H., Isralewitz, B., Krammer, A., Vogel, V., and Schulten, K. 1998. Unfolding of titin immunoglobulin domains by steered molecular dynamics simulation. *Biophys. J.* **75:** 662–671.
Marszalek, P.E., Lu, H., Li, H., Carrion-Vazquez, M., Oberhauser, A.F., Schulten, K., and Fernandez, J.M. 1999. Mechanical unfolding intermediates in titin modules. *Nature* **402:** 100–103.
Merkel, R., Nassoy, P., Leung, A., Ritchie, K., and Evans, E. 1999. Energy landscapes of receptor–ligand bonds explored with dynamic force spectroscopy. *Nature* **397:** 50–53.
Nosé, S. 1984. A molecular dynamics method for simulations in the canonical ensemble. *Mol. Phys.* **52:** 255–268.
Oberhauser, A.F., Hansma, P.K., Carrion-Vazquez, M., and Fernandez, J.M. 2001. Stepwise unfolding of titin under force-clamp atomic force microscopy. *Proc. Natl. Acad. Sci.* **98:** 468–472.
Paci, E. and Karplus, M. 1999. Forced unfolding of fibronectin type 3 modules: An analysis by biased molecular dynamics simulations. *J. Mol. Biol.* **288:** 441–459.
———. 2000. Unfolding proteins by external forces and high temperatures: The importance of topology and energetics. *Proc. Natl. Acad. Sci.* **97:** 6521–6526.
Paci, E., Caflisch, A., Plückthun, A., and Karplus, M. 2001. Forces and energetics of hapten–antibody dissociation: A biased molecular dynamics study. *J. Mol. Biol.* **314:** 589–605.
Paci, E., Vendruscolo, M., Dobson, C.M., and Karplus, M. 2002. Determination of a transition state at atomic resolution from protein engineering data. *J. Mol. Biol.* **324:** 151–163.
Pande, V.S., Baker, I., Chapman, J., Elmer, S.P., Khaliq, S., Larson, S.M., Rhee, Y.M., Shirts, M.R., Snow, C.D., Sorin, E.J., et al. 2003. Atomistic protein folding simulations on the submillisecond time scale using worldwide distributed computing. *Biopolymers* **68:** 91–109.
Ros, R., Schwesinger, F., Anselmetti, D., Kubon, M., Schäfer, R., Plückthun, A., and Tiefenauer, L. 1998. Antigen binding forces of individually addressed single-chain Fv antibody molecules. *Proc. Natl. Acad. Sci.* **95:** 7402–7405.
Ryckaert, J.-P., Ciccotti, G., and Berendsen, H.J.C. 1977. Numerical integration of the Cartesian equations of motion of a system with constraints: Molecular dynamics of *n*-alkanes. *J. Comput. Phys.* **23:** 327–341.
Schwesinger, F., Ros, R., Strunz, T., Anselmetti, D., Güntherodt, H.J., Honegger, A., Jermutus, L., Tiefenauer, L., and Plückthun, A. 2000. Unbinding forces of single antibody-antigen complexes correlate with their rates. *Proc. Natl. Acad. Sci.* **97:** 9972–9977.
Vendruscolo, M., Paci, E., Dobson, C.M., and Karplus, M. 2001. Three key residues form a critical contact network in a protein folding transition state. *Nature* **409:** 641–645.
Wagner, C. and Kiefhaber, T. 1999. Intermediates can accelerate protein folding. *Proc. Natl. Acad. Sci.* **96:** 6716–6721.
Wodak, S.J. and Janin, J. 2002. Structural basis of macromolecular recognition. *Adv. Prot. Chem.* **61:** 9–73.
Wu, L.C., Tuot, D.S., Lyons, D.S., Garcia, K.C., and Davis, M.M. 2002. Two-step binding mechanism for T-cell receptor recognition of peptide MHC. *Nature* **418:** 552–556.